




CONSTRUCTING MATHEMATICAL MODELS FROM SMALL DATA SETS: CELL-VIABILITY MODEL OF MELANOMA UNDER INHIBITION BY MAZ-51

ROUMEN ANGUELOV^{1,*} , CHARLISE BASSON², PRIYESH BIPATH²,
YVETTE HLOPHE², CAROLYN NADASEN³ , AVULUNDIAH EDWIN PHIRI¹
AND JUNE SEREM³ 

Abstract. The synthetic indolinone derivative MAZ-51 is a selective inhibitor of vascular endothelial growth factor receptor 3 (VEGFR-3), a tyrosine kinase receptor essential for lymphangiogenesis and tumor progression. By competing with adenosine triphosphate (ATP) for VEGFR-3 binding, MAZ-51 blocks VEGF-C activity, thereby suppressing melanoma cell proliferation and promoting apoptosis. In this study, we employ mathematical modelling to quantify the inhibitory effects of MAZ-51 on the growth of B16-F10 melanoma cells. Cell viability is modeled as a function of both treatment duration and inhibitor concentration, providing a dynamic framework for assessing therapeutic efficacy. Our approach addresses a central challenge in mathematical biology: developing models that remain interpretable and predictive despite limited and variable data. By integrating biological insight with experimental data, we derive a parsimonious model that avoids overparameterization and yields biologically meaningful parameters. The model allows straightforward computation of pharmacological measures such as the half-maximal inhibitory concentration (IC_{50}) and provides deeper insight into the growth rate reduction of melanoma cells under VEGFR-3 inhibition. This work highlights the utility of mathematical modelling in elucidating drug action mechanisms and in quantitatively evaluating targeted cancer therapies.

Mathematics Subject Classification. 37N25, 92B05, 92C37, 92C50.

Received May 3, 2025. Accepted November 20, 2025.

1. INTRODUCTION

This study employs mathematical modelling to investigate how the synthetic indolinone derivative MAZ-51 (3-(4dimethylamino-naphthelen-1-ylmethylene)-1,3-dihydroindol-2-one) inhibits the growth of B16-F10 melanoma cells. Vascular endothelial growth factor receptor 3 (VEGFR-3), a tyrosine kinase receptor, plays a central role in lymphangiogenesis and tumour progression. MAZ-51 acts as an ATP-competitive inhibitor of VEGFR-3,

Keywords and phrases: Cell viability, mathematical model, cancer inhibition, melanoma, MAZ-51.

¹ Department of Mathematics and Applied Mathematics, University of Pretoria, South Africa.

² Department of Physiology, University of Pretoria, South Africa.

³ Department of Anatomy, University of Pretoria, South Africa.

* Corresponding author: roumen.anguelov@up.ac.za

blocking its autophosphorylation and thereby suppressing VEGF-C-mediated signaling. This inhibition disrupts vascular and lymphatic endothelial proliferation and may also reduce melanoma cell viability by inducing apoptosis.

B16-F10, a highly metastatic murine melanoma cell line syngeneic to C57BL/6 mice, is extensively used for preliminary screening of antitumour agents. *In vitro* assays typically evaluate cell viability, proliferation, apoptosis, migration, and invasion following treatment with candidate compounds [1, 2]. The B16-F10 *in vitro* experiments are often the approach of choice in melanoma research that provides for rapid screening of drug candidates in the setting of reduced complexity, *i.e.* isolating the direct effect of a drug on cancer cells, separate from the systemic influences of an animal, [3]. Data from *in vitro* experiments are used to justify, design, and dose subsequent animal studies, making the overall drug development pipeline more efficient and ethically sound, [4]. In a study using B16-F10 cells, [5], it is demonstrated that sodium dichloroacetate (DCA) significantly reduced B16-F10 proliferation and induced apoptosis, supporting its potential as a repurposed anticancer drug. Similarly, systematic reviews confirm that B16 sublines provide reliable, reproducible data for assessing dose-dependent cytotoxicity, cell-cycle arrest, and modulation of key pathways such as Phosphoinositide 3-kinase/Protein kinase B (PI3K/Akt) and mitogen-activated protein kinase (MAPK) [6].

In vivo B16-F10 models offer a physiologically relevant system to evaluate antitumour efficacy, metastasis inhibition, and host responses. The cell lines compatibility with immunocompetent C57BL/6 mice allows assessment of immune-tumour interactions and systemic toxicity. Common models include subcutaneous tumour implantation to monitor tumour growth inhibition and intravenous injection to study lung metastasis. The protocol for the use of B16 melanoma for clinical studies has been described by [7]. In [5] it is reported that DCA treatment significantly attenuated tumour progression in B16-F10-bearing mice, mirroring its *in vitro* effects. Complementary evidence from [6] shows that numerous plant-derived compounds similarly reduced tumour volume and metastatic nodules in B16-F10 models, highlighting the systems robustness for preclinical therapeutic screening.

Together, *in vitro* and *in vivo* B16-F10 experiments form a translational pipeline that strengthens preclinical efficacy testing for candidate melanoma therapies. Mathematical modelling, particularly agent-based modelling as highlighted by [8], complements these approaches by enabling the integration and interpretation of data across experimental systems. Such models help validate and contextualise *in vitro* findings, inform the design and dosing strategies of *in vivo* studies, and predict treatment outcomes under different experimental conditions. Mathematical modelling reduces unnecessary animal use, enhances experimental reproducibility, and improves the overall translational reliability of preclinical studies, thereby aligning with ethical and scientific standards.

The focus of this paper is assessing the inhibitory effect of MAZ-51 on B16-F10 melanoma cells. More precisely, the goal is to quantify, analyse and characterise the impact over time of varied concentrations of MAZ-51. Cell viability is used as a quantitative measure of treatment efficacy. It is defined as the size of a drug-treated cell population expressed as a percentage of the size of an untreated, naturally growing population. Determining cell viability as a function of both time and drug concentration is an important step in the development of effective cancer therapies and is the approach followed here. This investigation is part of a broader ongoing research project on inhibition of melanoma, with some results on other inhibitors already reported in [9, 10].

Measurements of the cell viability over time for different concentration of the inhibitor are obtained through *in vitro* experiments. Building mathematical models that captures accurately the inhibition processes presents significant challenges, not uncommon for modeling of biological systems. Indeed, biological systems are complex, experimental data are often limited, and variability across cell populations can exceed the explanatory power of any single model. Overly complex models risk overparameterization, weak identifiability, and unstable parameter estimates, which in turn can obscure mechanistic interpretation and reduce predictive reliability.

To address these challenges, our work emphasises model parsimony and biological interpretability. Since our *in vitro* experiments directly measure melanoma cell viability under varying concentrations of MAZ-51, we construct a model in which cell viability is the sole observable variable. The model incorporates only the most essential processes governing treatment response, with parameter values estimated through iterative refinement between experimental data and model structure.

By balancing biological realism with mathematical tractability, this approach yields a model that is both mechanistically informative and practically predictive. Our results provide insights into the time evolution of the inhibition process under varied concentration of MAZ-51 and offer a framework for quantitatively evaluating its therapeutic efficacy.

The structure of the paper is as follows. In the next section, we discuss the pharmacological profile of MAZ-51, the experimental design and the obtained data as well as the variability that cannot be explained by any model in which only time and concentration are considered independent variables. Consequently, the dataset relevant to the model is smaller than it initially appears. This observation motivates a minimalistic modeling approach that focuses on representing only the most impactful processes. In Section 3 we derive a general form of the model. In Section 4 we associate the model with the data, where on the one hand, the structure of the model is refined, and on the other hand, the values of the parameters are identified. The robustness of the parameter identification is shown through the uniqueness of the values minimizing the least squares objective function. Discussion regarding the interpretation of parameters, deriving biologically interpretable quantities, such as the growth rate reduction of the cancerous cell population in response to MAZ-51 as well as straightforward computation of standard pharmacological measures, including the half-maximal inhibitory concentration (IC_{50}) is presented in Section 5. Section 6 gives some concluding remarks regarding the significance of the modeling approach and the obtained results.

2. *In vitro* EXPERIMENTS AND DATA

2.1. MAZ-51 pharmacological profile

MAZ-51, a selective VEGFR-3 (vascular endothelial growth factor receptor-3) tyrosine kinase inhibitor, has garnered significant attention as an anti-proliferative and anti-angiogenic agent in cancer therapeutics [11]. Its activity against melanoma, a highly aggressive and vascularised malignancy, is interlinked *via* many molecular and cellular mechanisms that make it a good candidate for therapeutic application. These mechanisms span angiogenesis inhibition, cell cycle regulation, adhesion and migration interference, and synergistic modulation with phytochemicals.

The primary pharmacological target of MAZ-51 is VEGFR-3, a receptor tyrosine kinase predominantly expressed on lymphatic endothelial cells and aberrantly upregulated in various tumour types, including melanoma. In [12] it is demonstrated that VEGF-C signalling through VEGFR-3 significantly enhances melanoma cell adhesion, proliferation, and migration, partly through the upregulation of CXCR4 (C-X-C chemokine receptor 4) and reciprocal activation of VEGF-C/VEGFR-3 autocrine loops. These pathways drive tumour invasiveness and metastatic dissemination through both angiogenic and lymphangiogenic mechanisms. By selectively inhibiting VEGFR-3 phosphorylation, MAZ-51 disrupts these autocrine loops, thereby impairing VEGF-C-driven endothelial and melanoma cell interactions and reducing vascular permeability and neo-lymphatic vessel formation [12]. This suppression of VEGFR-3 signalling translates into reduced nutrient and oxygen delivery to melanoma tissues, effectively starving tumour cells and limiting their proliferative capacity.

Furthermore, MAZ-51 interferes with VEGFR-3 downstream signalling pathways [13], such as PI3K/Akt and extracellular signal-regulated kinases 1 and 2 (ERK1/2), which are critical for melanoma survival and motility [14]. Inhibiting these cascades contributes to reduced phosphorylation of survival proteins, promoting apoptotic signalling and diminishing the tumour's angiogenic potential.

MAZ-51 has been shown to exert direct anti-proliferative effects on melanoma cells independent of its vascular effects. In [15] it is demonstrated that MAZ-51 treatment led to G2/M phase arrest in human melanoma cell lines, accompanied by a reduction in cyclin B1 and Cdc2 (CDK1) expression. This indicates interference with the mitotic entry checkpoint, effectively halting cell cycle progression. Moreover, exposure to MAZ-51 enhanced caspase-3 activation and PARP cleavage, hallmarks of apoptotic induction. These findings align with the compound's ability to disrupt VEGFR-mediated pro-survival signalling, particularly through PI3K/Akt pathway inhibition. The resulting decrease in anti-apoptotic B-cell lymphoma 2 (Bcl-2) family proteins and increase in pro-apoptotic Bcl-2-associated X protein (Bax) further underscores its intrinsic cytotoxic potential against melanoma cells [15].

Melanoma metastasis depends heavily on adhesion molecule dynamics and cytoskeletal rearrangements, both regulated by growth factor signalling. [12] elucidated that VEGF-C stimulation promotes integrin-mediated adhesion in both melanoma and endothelioma cells, a process that fosters metastatic colonization. MAZ-51 effectively inhibits these adhesive interactions by blocking VEGFR-3 activation, thereby reducing the recruitment of focal adhesion kinase (FAK) and other scaffolding proteins necessary for cell migration and attachment. This anti-adhesive property of MAZ-51 is particularly relevant in preventing tumour cell–endothelium interactions that precede intravasation and metastasis. Inhibition of adhesion not only diminishes metastatic potential but also enhances chemosensitivity, as the detachment of cells from the extracellular matrix can trigger anoikis, a form of apoptosis induced by loss of adhesion [15]. MAZ-51’s pharmacological profile confers several translational advantages for melanoma therapy. Its selectivity toward VEGFR-3 minimizes off-target inhibition of VEGFR-1/2, thereby reducing systemic side effects typically associated with pan-VEGF inhibitors [13]. Moreover, its lipophilic structure facilitates cell membrane penetration, allowing it to exert both extracellular and intracellular actions in melanoma cells.

As noted in [15], MAZ-51 exhibited favourable cytotoxic profiles at micromolar concentrations with a marked therapeutic window between melanoma and non-tumorigenic cells, indicating selective toxicity. This differential sensitivity supports its feasibility for targeted interventions, especially when delivered through nanoparticle carriers or combination regimens to enhance bioavailability and reduce systemic exposure.

Beyond its direct cellular effects, MAZ-51 modulates the tumour microenvironment (TME) by inhibiting endothelial cell proliferation, reducing vascular permeability, and attenuating pro-inflammatory cytokine secretion. Inhibition of VEGFR-3 in both endothelial and tumour compartments can decrease immune evasion mechanisms, thereby improving infiltration of cytotoxic T cells and enhancing the immune-mediated anti-tumour response. The compound’s ability to impact both vascular and immune axes of tumour growth positions it as a dual-action inhibitor, bridging angiostatic and immunomodulatory therapies in melanoma [12, 14]. The anti-melanoma potential of MAZ-51 is derived from its multi-targeted inhibition of VEGFR-3–driven signalling, cell cycle arrest, pro-apoptotic induction. Its dual inhibition of tumour and endothelial cell pathways, coupled with favourable selectivity and translational feasibility, underscores its promise as a viable compound for melanoma inhibition.

2.2. Crystal violet assay for MAZ-51 inhibition

B16-F10 murine melanoma cells were exposed to MAZ-51 at concentrations of 11 μM , 13 μM , 14 μM and 16 μM for 24, 48 and 72 hours. The goal was to measure the effect of the inhibitory agent on cell viability. For each concentration and time point, **cell viability** is defined as the ratio of the size of the treated population to the size of the corresponding untreated population.

Experimentally, the cell viability is measured using the crystal violet assay as follows. B16-F10 cells were seeded at a density of 5000 per well in 96 well plates in complete culture medium, consisting of Dulbecco’s modified essential medium, 10% fetal calf serum and 1% antibiotics (amphotericin/penicillin/streptomycin). The cells were incubated in a humidified Forma Scientific water-jacketed incubator at 37°C with 5% CO₂ overnight to allow the cells to adhere to the plate. The following day, the cells were exposed to the compound at varying concentrations. Each experimental repeat included a vehicle control group (no inhibition) and groups treated with varied concentrations of the inhibiting agent. At least 9 wells from each group were analyzed in 24 hours, 48 hours, and 72 hours. The experiments were terminated by fixing the cells with 2% (v/v) formaldehyde for 30 minutes and then stained with 100 μL of 0.1% crystal violet in 0.75 mM formic acid for 30 minutes. The crystal violet dye stains only the nuclei of living cells. The wells were washed with tap water and dried. Then the absorbance of the dye is measured using a spectrophotometer at 630 nm upon adding 100 μL of 10% (v/v) acetic acid to each well. The size of cell population is strongly and positively correlates with dye absorbance. Hence, the cell viability is calculated as the absorbance of the treated population divided by the absorbance of the control population. Note that the cell viability is a non-dimensional variable usually expressed as a percentage.

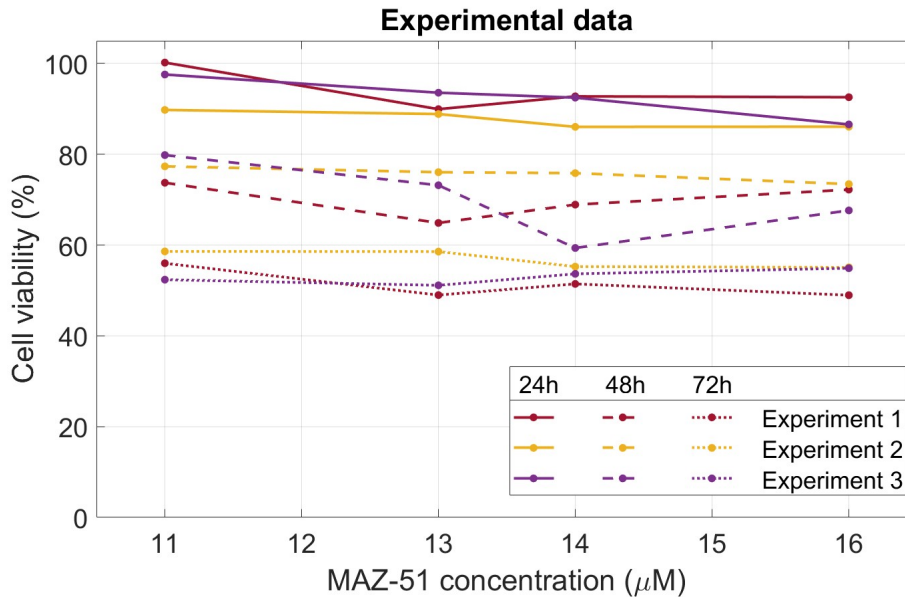


FIGURE 1. Values of cell viability at 24 h (data points connected by solid line), 48 h (points connected by dashed line) and 72 h (data points connected by dotted line) for MAZ-51 concentrations of 11 μM , 13 μM , 14 μM and 16 μM . Experiments are repeated three times.

Since each well was measured only once, replicate wells at the same inhibitor concentration and same time point exhibit variability, reflecting experimental noise and biological heterogeneity. As an illustration, Figure 1 presents cell viability data from three independent experimental runs of the crystal violet assay for MAZ-51 concentrations of 11 μM , 13 μM , 14 μM , and 16 μM . In the Section 2.3 we show mathematically that this variability cannot be explained by any model having only time and concentration as independent variables and that in actual fact we have far fewer data points than the ones plotted on Figure 1. More precisely, any model based on least squares fit approximates the means of the data for any fixed concentration and time point, that is only the data presented on Figure 2.

2.3. Limitations of least squares approximation of data clustered at few values of the model variable(s)

We consider the least squares approximation of data sets of the type described in the preceding subsection in the following more general setting. We assume that a process $w(v)$, depending on the variable v , which is possibly multidimensional, is observed repeatedly and measurements are taken at distinct points $\{v_j : j \in J\}$, where J is a given index set. Further, assume that at the point v_j we have m_j measurements denoted by $w_{1j}, w_{2j}, \dots, w_{m_j j}$, $j \in J$. Denote by \bar{w}_j the mean of the measurements at v_j , that is

$$\bar{w}_j = \frac{1}{m_j} \sum_{i=1}^{m_j} w_{ij}.$$

We consider the approximation of the data

$$\{w_{ij} : i = 1, \dots, m_j, j = 1, \dots, n\} \quad (2.1)$$

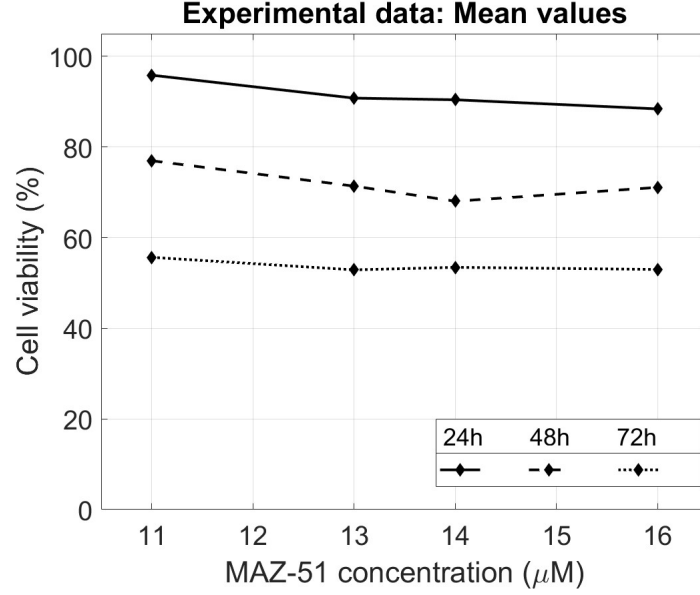


FIGURE 2. Mean values of cell viability at 24 h (data points connected by solid line), 48 h (points connected by dashed line) and 72 h (data points connected by dotted line) for MAZ-51 concentrations of 11 μM , 13 μM , 14 μM and 16 μM .

by a function of v , $\varphi(a, v)$, which depends on a vector of parameters a . The Least Squares Method yields an approximation $\varphi(\hat{a}, t)$, where \hat{a} minimizes the sum of the squared deviations, that is

$$\Psi(a) = \sum_{j \in J} \sum_{i=1}^{m_j} (\varphi(a, t_j) - w_{ij})^2. \quad (2.2)$$

Considering that we have multiple data points for every point v_j , the following Lemma is useful.

Lemma 2.1. *Let $k \in \mathbb{N}$ and let z, y_1, y_2, \dots, y_k be real numbers. Then*

$$\sum_{i=1}^k (z - y_i)^2 = k(z - \bar{y})^2 + \sum_{i=1}^k (y_i - \bar{y})^2,$$

where $\bar{y} = \frac{1}{k} \sum_{i=1}^k y_i$.

Proof.

$$\begin{aligned} \sum_{i=1}^k (z - y_i)^2 &= kz^2 - 2z \sum_{i=1}^k y_i + \sum_{i=1}^k y_i^2 \\ &= kz^2 - 2kz\bar{y} + k\bar{y}^2 + \sum_{i=1}^k y_i^2 - 2\bar{y} \sum_{i=1}^k y_i + k\bar{y}^2 \\ &= k(z - \bar{y})^2 + \sum_{i=1}^k (y_i - \bar{y})^2. \end{aligned}$$

□

Using Lemma 2.1, the sum of the squared deviations (2.2) can be represented in the form

$$\Psi(a) = \sum_{j \in J} m_j (\varphi(a, v_j) - \bar{x}_j)^2 + \sum_{j \in J} \sum_{i=1}^{m_j} (w_{ij} - \bar{w}_j)^2$$

The value of the second sum, namely

$$IRE = \sum_{j \in J} \sum_{i=1}^{m_j} (x_{ij} - \bar{x}_j)^2, \quad (2.3)$$

does not depend on the function φ and the parameter a . Hence, it represents an irreducible error for the Least Squares approximation. Only the first sum,

$$\Phi(a) = \sum_{j \in J} m_j (\varphi(a, v_j) - \bar{w}_j)^2. \quad (2.4)$$

depends on φ and a and represents reducible error. Minimizing Ψ is equivalent to minimizing Φ . This shows that any minimizer \hat{a} is determined only by the mean values \bar{w}_j , $j \in J$, and not by the entire data set. Since $\{v_j : j \in J\}$ are different values of v , potentially $\Phi(\hat{a})$ can be zero, so that the change in \bar{w}_j , $j \in J$, could be fully explained by the model $\varphi(\hat{a}, v)$ through the change in v . However, clearly the model cannot explain the variation at any fixed v_j .

We collect the obtained results in the next theorem.

Theorem 2.2. *For the least squares approximation of the data set (2.1) by function $\varphi(a, t)$ depending on the parameter a , we have that \hat{a} is a minimizer of the sum of the squared deviations $\Psi(a)$ given in (2.2) if and only if \hat{a} is a minimizer of $\Phi(a)$ given in (2.4). Further we have*

$$\Psi(a) = \Phi(a) + IRE,$$

where IRE , as given in (2.3), depends on the data set only and not on a or φ .

This theorem can be applied to the experimental data described in Section 2.2 in different ways. Let the w be the cell viability, which is function of the time t and the inhibitor concentration x . Then we have $v = (x, t)$, $w(v) = w(x, t)$. Denote $t_1 = 24$, $t_2 = 48$, $t_3 = 72$ and $x_1 = 11$, $x_2 = 13$, $x_3 = 14$ and $x_4 = 16$. Then $J = \{1, 2, 3\} \times \{1, 2, 3, 4\}$ and the data set is

$$\{w_{ij} : i = 1, 2, 3, j \in J\} = \{w_{ikl} : i = 1, 2, 3, k = 1, 2, 3, l = 1, 2, 3, 4\},$$

where w_{ikl} is a measurement of $w(t_k, x_l)$. The theorem can also be applied for a fixed x , so that $v = t$, or for a fixed t , so that $v = x$.

Remark. Theorem 2.2 shows that the number of measurements taken at a fixed value v_j of the model variable v does not contribute to reliable and stable identifiability of the parameters, since only the mean value is used in the minimization of the least squares objective function. However, it strongly impacts the quality/reliability of (v_j, \bar{w}_j) as a data point. More precisely, assuming that the measurements $w_{1j}, w_{2j}, \dots, w_{m_j j}$ are a sample from the population of all measurements of $w(v_j)$, then using a statistical argument, the sample mean \bar{w}_j is a better approximation of the population mean when m_j is large.

3. MATHEMATICAL MODEL

We consider first a model for the growth of the control cell populations, that is, when the cells are provided with optimal growth conditions as described in Section 2.2 and not subjected to inhibition. Under these conditions, the population can be modelled *via* constant growth rate model, [16], Table 1, [17], Table 1, equation (20), [18], equation (1),

$$\frac{dP}{dt} = rP, \quad (3.1)$$

where $P(t)$ is the size of the population at time t and r is the constant relative growth rate per unit time. The solution of (3.1) is $P(t) = P(0)e^{rt}$. Hence, (3.1) is also called exponential growth model. This model is applicable while the stated optimal growth conditions prevail. Considering the experimental setting described in Section 2.2, we can assume that the growth conditions remain unchanged for the relatively short period of the experiments and, therefore, use the model (3.1) to represent the growth of the control population.

The effect of cancer treatment is typically modeled as a reduction of the growth rate, [16], [18], [17]. Considering the simplicity of the model (3.1), we apply the so called "log-kill" pattern, [19], [18], equation (7), [17], equations (21) and (22), that is, the growth rate of the inhibited population is given in the form $r - h$, where h represents the impact of the inhibition. Here h is a function of the time t and of the concentration x of the inhibitor. One can expect that with time the inhibitor binds with the cells, thus reducing the concentration of the free inhibitor. However, considering that the inhibitor significantly outnumbers the cell population in terms of molecules per cell, it can be expected that inhibition process does not have a measurable impact on the concentration of the inhibitor over the relatively short period of the experiments. Hence, we assume that in each experiment x is a constant. Specifically, it does not depend on t .

Let $Q(x, t)$ denote the size at time t of a cell populations treated by concentration x of the inhibitor, provided all other conditions are the same as for the control population. Then Q satisfies the equation

$$\frac{\partial Q(x, t)}{\partial t} = (r - h(x, t))Q(x, t). \quad (3.2)$$

Taking into account that the initial population of treated and control wells are the same, the solution of (3.2) is

$$Q(x, t) = P(0)e^{rt - \int_0^t h(x, \theta)d\theta}. \quad (3.3)$$

Then, from the definition of cell viability given in Section 2.1 it follows that the cell viability at time t under inhibitor concentration x is the function

$$\varphi(x, t) = \frac{Q(x, t)}{P(t)} = e^{-\int_0^t h(x, \theta)d\theta}. \quad (3.4)$$

We should mention that the dependence of h on t in cancer models, it usually represents change of treatment/dose/concentration, [18]. For example, in [20] the dependence on t of the right-hand side of the differential equation model represent an "on-off" switch of treatment. In such cases, the resulting model is not an autonomous system. In a contradistinction, the experiments described in Section 2.2 represent completely autonomous population growth, in the sense that there is no external input for entire duration of the experiment, namely from setting the wells until termination of the process for measurement of the cell viability at that time point. Therefore, the dependence of h on t represents the evolution of the inhibition rate with time.

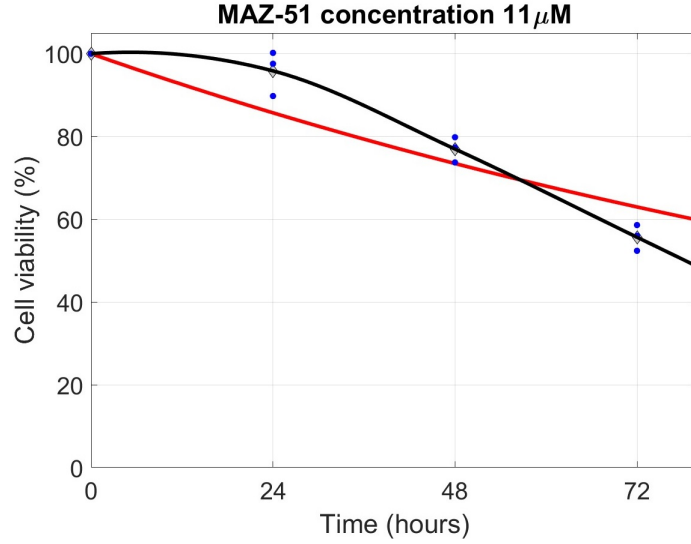


FIGURE 3. Values of cell viability under concentration $11 \mu\text{M}$ of the inhibitor measured at 24 h, 48 h and 72 h (blue dots). The graph of the best fitting exponential decay function is given as a red line. We have $R^2 = 84.15\%$ – a rather low value. Further, the qualitative mismatch with the graph (black line) of the cubic spline interpolating the mean values (grey diamonds) of the data is apparent.

It was established experimentally and theoretically in [9, 10] that the inhibition rate may vary with time, specifically, increasing from 0 to some maximal value. Such temporal dynamics are also suggested by the experimental data presented here for MAZ-51 inhibition. Indeed, if h is independent of t , the cell viability function (3.4) would represent exponential decay. Figure 3, representing the data for concentration $x = 11 \mu\text{M}$ and the best fitting exponential decay curve, illustrates that exponential decay model does not capture well the time evolution of the cell viability for given x . For comparison the cubic spline interpolating the mean values of the data at any time point is plotted on the same figure. This spline is the simplest piece-wise polynomial function which has a smooth derivative and passes through the stated points. Its graph shows that any sufficiently well fitting to the data curve is concave down in some initial period before it reaches a point of inflection and is concave up thereafter. This shape is consistent with h being increasing on t from 0 to some maximal value. In a contradistinction, the exponential decay curve is concave up over the whole real line.

A suitable candidate for parametrization of h such that $h(x, 0) = 0$ and $h(x, t)$ is increasing with respect to time towards some maximal value, $m(x)$ is the function

$$h(x, t) = m(x) \left(1 - e^{-\lambda(x)t}\right), \quad (3.5)$$

where $\lambda(x)$ is a positive function of x . Evaluating the integral in (3.4) we obtain

$$\varphi(x, t) = e^{-m(x) \left(t + \frac{e^{-\lambda(x)t} - 1}{\lambda(x)}\right)}. \quad (3.6)$$

Let us note that the functions φ and h satisfy the system

$$\frac{d\varphi(x, t)}{dt} = -h(x, t)\varphi(x, t) \quad (3.7)$$

$$\frac{dh}{dt} = \lambda(x)(m(x) - h(x, t)). \quad (3.8)$$

For every x the system (3.8)-(3.7) is an autonomous system of differential ordinary equations, which reflects the autonomous character of the experiments discussed earlier. Further, from (3.8)-(3.7) we obtain that

$$\frac{d^2\varphi(x, t)}{dt^2} = (h^2(x, t) + \lambda(x)h(x) - \lambda(x)m(x))\varphi(x, t).$$

It is easy to see, for a fixed x , that the continuous function $\gamma(x, t) = h^2(x, t) + \lambda(x)h(x) - \lambda(x)m(x)$ is increasing from a negative value $\gamma(x, 0) = -\lambda(x)m(x)$ to a positive value $\lim_{t \rightarrow +\infty} \gamma(x, t) = m^2(x)$ and, therefore, it changes sign from negative to positive at some point $t(\hat{x}) > 0$. Since the sign of the second derivative determines the concavity of a curve, we have that $\varphi(x, t)$ is concave down for $0 \leq t < \hat{t}(x)$ and concave up for $t > \hat{t}$, which is consistent with the expected time dynamics of φ discussed above.

4. ASSOCIATING THE MATHEMATICAL MODEL WITH THE EXPERIMENTAL DATA

We have data from three experimental repeats for each of the concentrations of MAZ-51, giving the cell viability at 24h, 48h and 72h. Taking into account also $t = 0$ where the cell viability is assumed to be 100%, we have 12 data values for every concentration, total of 48 data values that can be used to align the model (3.6) with the experimental measurements. However, the model (3.6) is constructed in such a way that $\varphi(x, 0) = 0$ for any x , m and λ . Further, the rest of the measurements are at three time points, namely 24 h, 48 h and 72 h, as stated above. The situation of fitting a time dependent model of data clustered at few time points is discussed in Section 2.2, where it is shown, see Theorem 2.2, that such model may not explain the variation at the individual time points and the model is in practice fitted to the means of the data at these time points. Hence, we have 12 data values to identify the parameters in the model (3.6), see Figure 2. In this regard, it is significant that the model of cell viability (3.6) is derived from biological insight in terms of two concentration dependent parameters only. Identifying these parameters is still a challenge, considering that m and λ are functions of x . In this section, we show how this challenge can be resolved so that the approximation makes sense from biological point of view and it is mathematically robust.

We express the accuracy of approximation in absolute terms, namely *via* the residual least squares error, SS_{res} (sum of the squared deviation of the model values from the measurements), and in relative terms through the coefficient of determination

$$R^2 = 1 - \frac{SS_{res}}{SS},$$

where SS is the sum of squares (sum of the squared deviations of all measurements from their mean).

As a first step we fit the model (3.6) to the data separately for each of the concentrations x and identify the values of m and λ for the specific concentration. The data (blue dots) and the fitted models (3.6) (dotted black lines) are given on Figure 4.

One can observe in the numerical results presented in Table 1 that the accuracy is very good with R^2 very close to 1 for all concentrations. One can also observe significant inconsistencies in the estimated values of the parameters. This is not really unexpected, considering that for every concentration two parameters are estimated from three data points. Specifically, at $x = 11 \mu\text{M}$ this is compounded with the fact for such small value of λ , we have

$$e^{-\lambda(x)t} \approx 1 - \lambda(x)t + \frac{1}{2}\lambda^2(x)t^2, \quad (4.1)$$

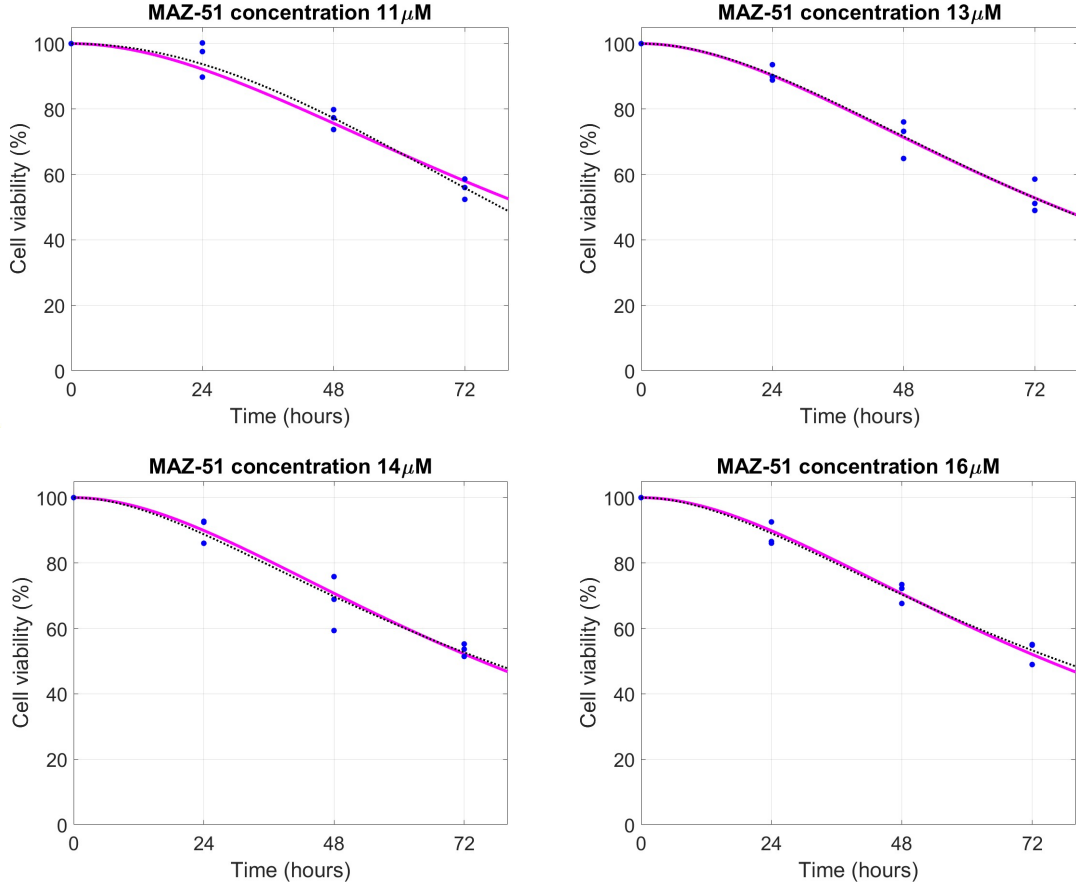


FIGURE 4. Fitting of the model independently for each concentration value. Blue dots represent the data points. Dotted black lines – unconstrained fit. Magenta solid lines – fit with monotonicity constraint on m and λ .

TABLE 1. Estimated values of the parameters m and λ and the error of approximation for each concentration.

Concentration	11 μM	13 μM	14 μM	16 μM
m	59.3785	0.0161	0.0126	0.0125
λ	3.7799e-06	0.0264	0.0460	0.0445
SS_{res}	0.0111	0.0130	0.0192	0.0072
R^2	0.9708	0.9681	0.9730	0.9813

and, consecutively,

$$\varphi(x, t) \approx \phi(x, t) := e^{-\frac{1}{2}m(x)\lambda(x)t^2}. \quad (4.2)$$

Therefore, only the product $m(11)\lambda(11)$ can be reliably estimated, but not $m(11)$ and $\lambda(11)$ separately. Note that $m(11)\lambda(11) = 2.2444e - 04$, which is within the range of the products of m and λ for the other concentrations.

TABLE 2. Estimated values of the parameters m and λ obtained *via* fitting the model to all data under monotonicity assumption for m and λ . The error of approximation is given for each concentration and overall over all concentrations. The same values correct to 4 decimal places are obtained under the assumption that m is a constant, that is, estimating 5 rather than 8 parameter values.

Concentration→ Parameters↓	11 μM	13 μM	14 μM	16 μM	Overall
m	0.0151	0.0151	0.0151	0.0151	
λ	0.0222	0.0292	0.0309	0.0309	
SS_{res}	0.0159	0.0131	0.0200	0.0079	0.05688
R^2	0.9581	0.9680	0.9523	0.9797	0.96465

Considering the biological meaning of $m(x)$ and $\lambda(x)$ as given through equation (3.5), it is reasonable to expect that these functions are nondecreasing functions of the concentration x . This is not consistently observed in Table 1, even if we discard the estimates for $x = 11 \mu\text{M}$. As a second step, and in order to take into account the expected monotonicity of m and λ , we consider least squares approximation by the model (3.6) at all data points under the constraint that m and λ are nondecreasing functions of x . The estimated values of m and λ are given in Table 2. As it can be expected, there is a decrease in accuracy of the fitting to the data, *e.g.* the R^2 values are all smaller than the respective values in Table 1. However, this decrease is very marginal. Specifically, all R^2 values are above 95%. The fitted curves are plotted as magenta solid lines on Figure 4.

The results suggest that m is independent of x . The biological meaning of this is that the maximum inhibition level is independent of the concentration of the inhibitor. For higher concentrations this maximum is approached faster, for lower concentrations - slower. Alternatively this means that the same level of inhibition may be reached using different concentrations, but at different times, with concentration and time being negatively correlated. Hence, it is biologically plausible and implied by the numerical approximation that m is a constant. We make this assumption in the sequel. As a next step we repeat the fitting of the model (3.6) to all data considering m being a constant. In this way, we estimate 5 parameter values, namely m , $\lambda(11)$, $\lambda(13)$, $\lambda(14)$ and $\lambda(16)$ using 12 data points. The obtained values for these parameters as well as the errors are the same correct to four decimals as in Table 2. However, having fewer parameter values to estimate make the optimization process more reliable.

The function λ is not yet derived in an explicit form as a function of the concentration x . Only estimates of the values for the concentrations involved in the experiments have been obtained. Including the origin, we have a total of five data points as plotted on Figure 5 (top, left). We can make a general observation that the function $\lambda(x)$ is increasing (already discussed) and it saturates at a level just above 0.03. There are a few functions used widely for describing biological growth that we can use. Here we consider the Von Bertalanffy function [21], the logistic function and the Gompertz function, [22–24]. Considering that $\lambda(0) = 0$, the three functions are

$$\lambda_1(x) = a \left(1 - e^{-c(1-b)x} \right)^{\frac{1}{1-b}} \quad (\text{Von Bertalanffy}) \quad (4.3)$$

$$\lambda_2(x) = a \frac{1 - e^{-cx}}{1 + be^{-cx}} \quad (\text{Logistic}) \quad (4.4)$$

$$\lambda_3(x) = a \left(1 - e^{b(1-e^{cx})} \right) \quad (\text{Gompertz}) \quad (4.5)$$

In all three models a is a scaling parameter for λ , c is a scaling parameter for x , and b (dimensionless) is a “shape” parameter. In (4.3) b is the so called Von Bertalanffy exponent, $0 \leq b < 1$. The parameters a and c are assumed positive. In (4.4) and (4.5) the value of b determines the horizontal shift of the standard logistic curve or Gompertz curve, respectively. The point of inflection of (4.4) is $x = \frac{\ln b}{c}$, while the point of inflection of (4.5) is $x = -\frac{\ln b}{c}$. Parameter b is positive for both models. Due to the symmetry of the logistic curve with

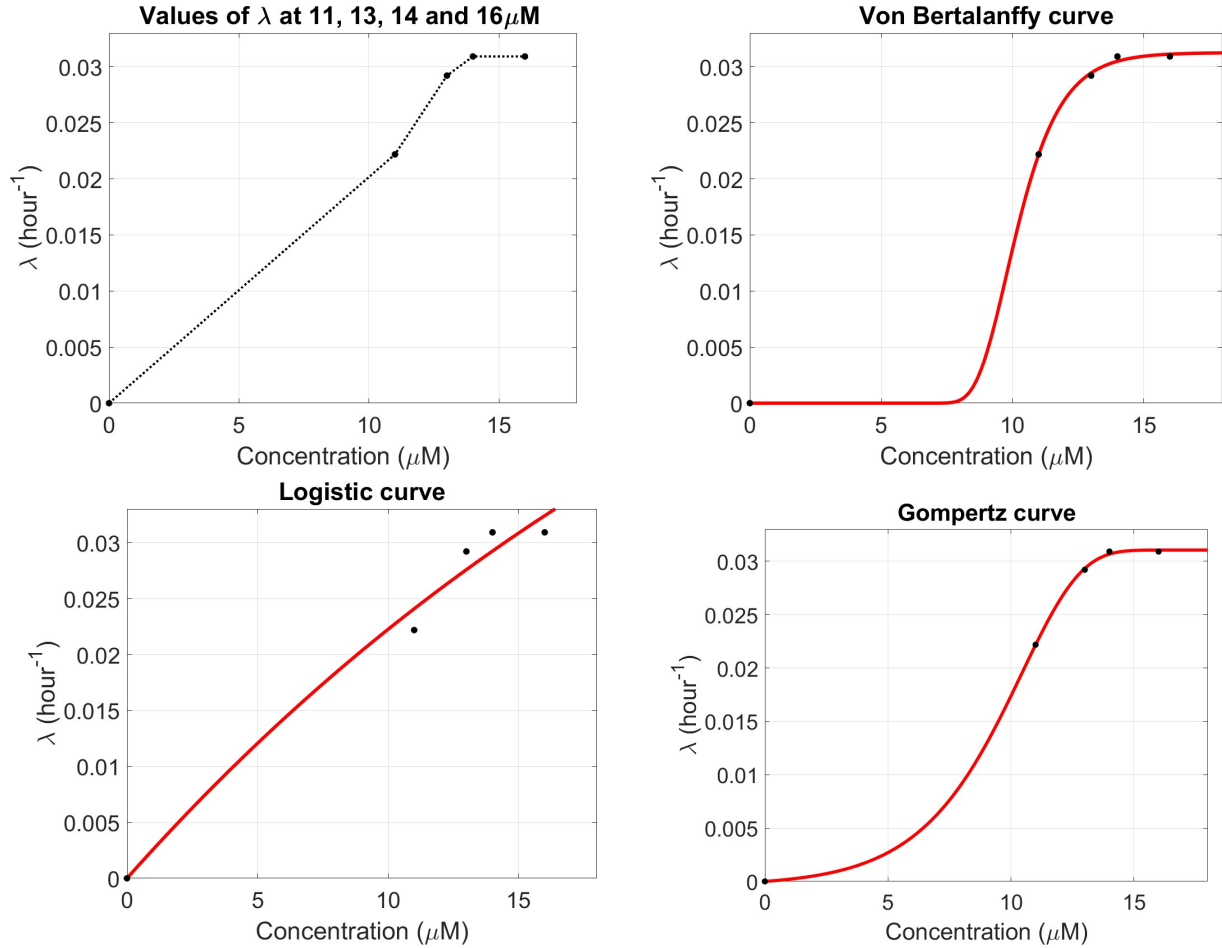


FIGURE 5. Computed values of λ for the tested concentrations and the curves of the form (4.3), (4.4), (4.5) fitted to them.

TABLE 3. Estimated values of the parameters a , b and c obtained for the models (4.3), (4.4) and (4.5) obtained *via* fitting these models to computed values for λ at 11 μM , 13 μM , 14 μM and 16 μM . Unrealistic estimates for some of the parameters of the Von Bertalanffy model and of the Logistic model are observed.

	a	b	c	SS_{res}	R^2
Von Bertalanffy	0.03125	0.99980	459.97	2.8064×10^{-7}	0.99959
Logistic	0.07755	5.8215×10^{-17}	0.03381	1.1279×10^{-5}	0.98372
Gompertz	0.03105	0.41634	0.01296	9.45757×10^{-8}	0.99986

respect to its inflection point, we can assume that a and c are positive. Since the Gompertz function does not have such symmetry, a and c in (4.5) are just real numbers. We establish in the sequel that the optimal values of the parameters a and c are positive, without any positivity constraint in the optimization problem.

We fit to the values of λ plotted on Figure 5 (top, left) the models (4.3), (4.4) and (4.5). The fitted curves are presented in the remaining three plots in Figure 5, while the values of the parameters are given in Table 3. The

accuracy in terms of SS_{res} and R^2 is very good for all three curves with the Gompertz curve providing nearly perfect fit. We make also the following observations.

- Von Bertalanffy model. The Von Bertalanffy exponent b is very close to 1. We can recall that if $b = 1$ the Von Bertalanffy differential equation is linear and the solution is an exponential function. Typical values of b are $\frac{2}{3}$, $\frac{3}{4}$, [21]. The graphical manifestation of b being close to 1 is that for a relatively long initial period the value of the function is almost zero. There is no reason to expect such rather unusual behaviour.
- Logistic model. The small value of b indicates that the denominator has little effect on the value of the function in the considered range. A good fit is obtained for saturation level a , which is much larger than the expected one.
- Gompertz model. The growth and the saturation level are consistent with the process of inhibition in terms of both biological insight and available data. This aligns well with the fact that the model provides near perfect fit to the λ values with $R^2 = 99.986\%$.

Hence, the Gompertz model is not only the best of the three, but it is also the only realistic one for the modelled process.

Our search was limited to three parameter functions. There are other biological growth functions, which involve more parameters, *e.g.* the Richard's function (also called the generalized logistic function), [22, 25]. However, considering the small amount of data points for λ , this is likely to result in overparameterization. Hence, we reduce the number of parameters to the possible minimum, namely three. The explanation of the meaning of a , b and c given earlier makes it is clear that the model of λ can not be expected to involve smaller number of parameters.

We proceed by taking the function $\lambda(x)$ as given in (4.5). In this way, we obtained the model (3.6) in the following explicit form

$$\begin{aligned} \varphi(x, t) &= e^{-m \left(t + \frac{e^{-at(1-e^{b(1-e^{cx}})} - 1)}{a(1 - e^{b(1-e^{cx}})}} \right)} \\ &= e^{-M \left(at - \frac{1 - e^{-at(1-e^{b(1-e^{cx}})}}{1 - e^{b(1-e^{cx}})} \right)}, \end{aligned} \quad (4.6)$$

where $M = \frac{m}{a}$. Since m is the maximal inhibition, measured in hours⁻¹, and a is growth rate of inhibition, measured in hours⁻¹, the parameter M is dimensionless. Further, a (in hours⁻¹) and c (in μM^{-1}) are, in fact, scaling parameters for time and concentration, so that at and cx are both dimensionless. Parameter b is dimensionless as mentioned earlier. Therefore, any re-scaling of time, *e.g.* hours to minutes, or any re-scaling of concentration, *e.g.* μM to mM , affects only the values of a and c , respectively, and not the value of φ or the values of any of the other parameters.

The form (4.6) was obtained through several steps involving approximation and biologically meaningful assumptions suggested by the experimental data. In fact, we already have estimates for the parameters. A potential problem with this approach is that there could be accumulation of errors from step to step. We avoid this by fitting the model (4.6) directly to the experimental data. The values of the parameters identified in the least squares fitting process are given in Table 4. Using these parameters one can calculate $m = Ma = 0.0151$ as well as that the values of $\lambda(x)$ at $x = 11, 13, 14, 16$ are 0.0221, 0.0295, 0.0306, 0.0308, respectively. These values are very close to the values obtained in Table 2, showing that while the model has been extended as a continuous function of x and the number of parameters reduced, the accuracy at specific concentrations remains almost as good as the accuracy given by the parameter values in Table 2.

The cell viability, being a function of two variables, the inhibitor concentration and the time, is graphically represented via surface plot given in Figure 6. One can observe that the surface passes through the cloud of experimental data points plotted as blue balls.

TABLE 4. Parameter values for model (4.6).

M	a	b	c	SS_{res}	R^2
0.4912	0.0308	0.0088	0.4514	0.05696	0.96459

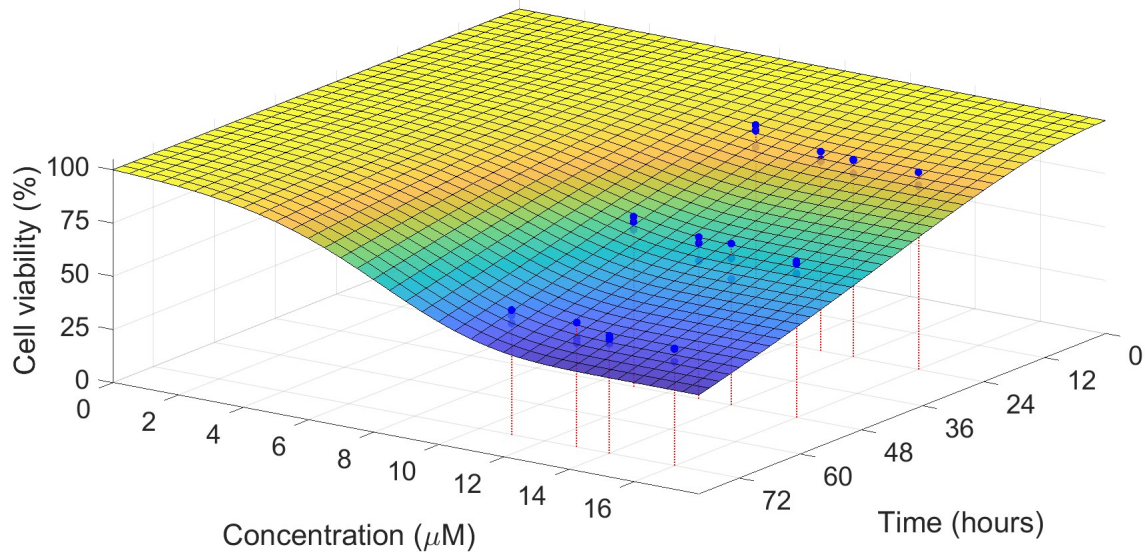


FIGURE 6. Surface plot of the cell viability as function time and concentration. Experimental data values given as blue balls.

From mathematical point of view the final model is obtained *via* two dimensional fit of the function (4.6) to the experimental data, where we estimate the values of four parameters using 12 data points. We may note that, at least in comparison to the first step, this is a fairly optimistic setting for reliable identification of the parameter values, particularly considering that the model (4.6) has been designed from biological insight and data analysis. Further, in solving numerically the minimization problem we observe that the objective function has a unique minimization point clearly identifiable with gradient decent methods initiated at any point. Hence, the optimization problem is well-posed and the parameter identification is robust.

5. DISCUSSION

The goal of the experimental work and of the theoretical analysis is ultimately to determine the efficacy of the inhibitor and possibly to suggest a protocol of treatment. The cell viability is an important concept capturing the inhibition properties of the tested compound. The model (4.6) with values of the parameters given in Table 4 was derived in the proceeding sections through integrating biological knowledge with experimental data. The function (4.6), being a continuous function of both variables, gives a predicted value for the cell viability at any time for any given concentration of the inhibitor. Hence, it provides a comprehensive overview of the potency of the inhibitor in terms of its concentration and of time.

Often experiments like the one considered in this paper are used to derive IC_{50} - the concentration of the inhibitor which yields cell viability of 50% at certain fixed time points, *e.g.* 48 h. The model (4.6) provides for computing IC_{50} at any time. More precisely, IC_{50} for a given time t is the solution x of the equation

$$\varphi(x, t) = 50. \quad (5.1)$$

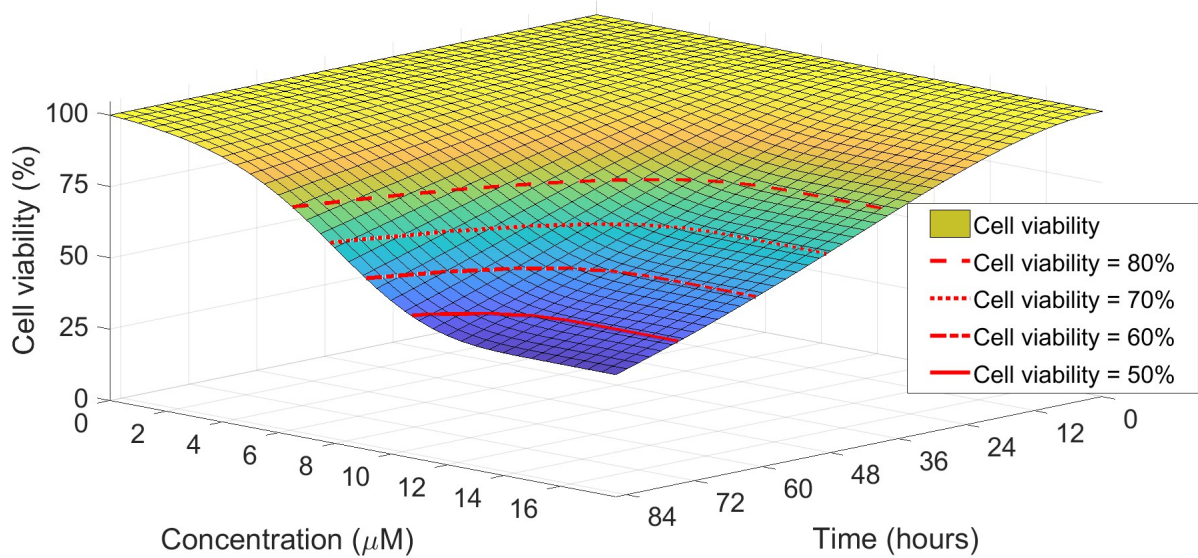


FIGURE 7. Surface plot of the cell viability as function time and concentration with level lines at 80%, 70%, 60% and 50%.

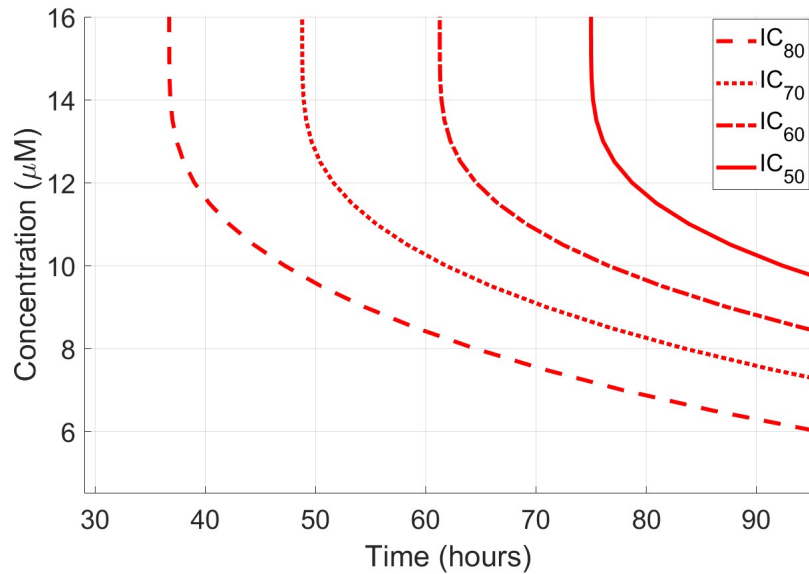


FIGURE 8. Inhibitory concentrations (IC) for cell viability of 80%, 70%, 60% and 50% as functions of time. The most commonly used IC_{50} is given by the solid line.

Mathematically, the equation (5.1) defines a level curve of the function φ , which implicitly defines x as a function of t . Further, we can consider level curves at any cell viability level. Level curves of cell viability at 80%, 70%, 60% and 50% are given on the surface plot in Figure 7. Two dimensional plots of these curves, concentration vs. time, are given in Figure 8, providing more insight into the impact of the inhibitor.

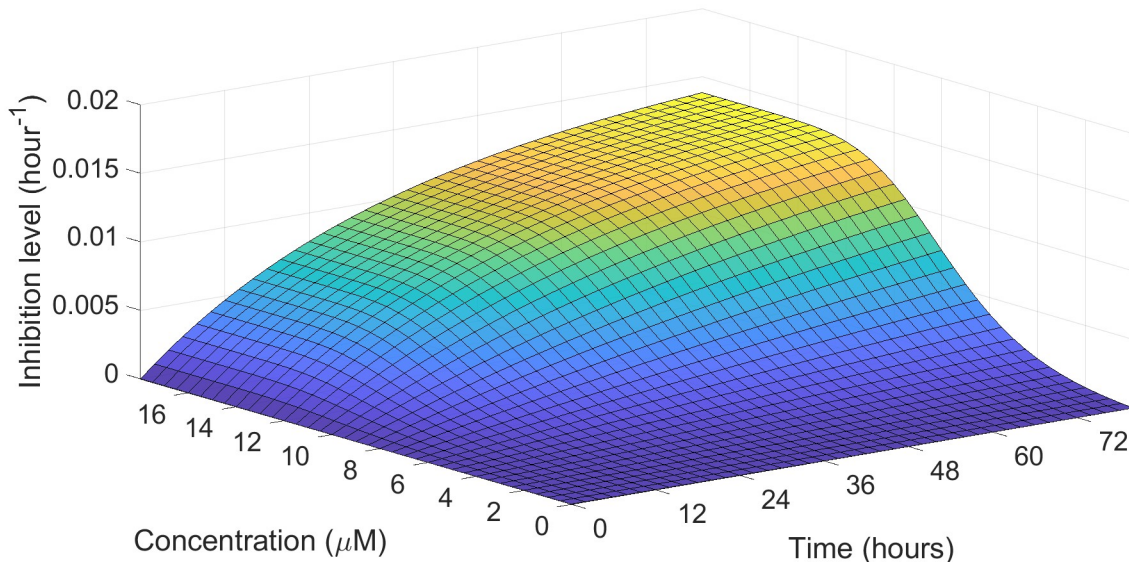


FIGURE 9. Surface plot of the level of inhibition as function of time and concentration.

Considering that the parameters of the model have specific biological meaning, one can derive other characteristics of the inhibition process, which can potentially provide useful insight into the inhibition dynamics. For example, we defined by $h(x, t)$ the level of inhibition, that is the amount by which the natural growth rate is reduced at time t due to the inhibitor concentration x . The level of inhibition is given by equation (3.5) or, equivalently, using (4.5), it is represented as

$$h(x, t) = m \left(1 - e^{at(1 - e^{b(1 - e^{cx})})} \right). \quad (5.2)$$

Surface plot of the function h with parameters as in Table 4 is presented in Figure 9.

6. CONCLUSION

Constructing useful mathematical models is typically guided by the objectives of (a) representing adequately the biological processes of interest; (b) identifying the values of the involved parameters. These two objectives are often in competition. On the one hand, due to the complexity of the biological processes, objective (a) leads to models involving many unknown parameters. On the other hand, only a limited number of variables can be measured, and obtaining these measurements requires costly, time-consuming, and labor-intensive experiments. The challenge is not new, Quoting Einstein: “It can scarcely be denied that the supreme goal of all theory is to make the irreducible basic elements as simple and as few as possible without having to surrender the adequate representation of a single datum of experience.” [26], p. 384.

In this paper we confront the competing objectives (a) and (b) in the setting of mathematical modelling of inhibition of melanoma. More precisely, we analyse the effect of the treatment of the B16-F10 melanoma cell line by MAZ-51 using the following protocol:

- Constructing a time-explicit model from biological insight about the inhibition process.
- Associating this model with the experimental data, which yields a reasonable extension to model of time and concentration.
- The two-dimensional model is fitted to all experimental data.

The reliability of the model stems from the fact that, on the one hand, it represents the available biological knowledge of the inhibition processes, and, on the other hand, it fits well the experimental data. Considering that the model uses only four parameters, the small least squares error is clearly not a result of "over-fitting". The observed numerical stability of the fitting process, namely a unique and clearly identifiable minimum of the objective function, indicates the robustness of the model.

The commonly used measure of inhibition efficacy, the IC_{50} at a given time, is easily derived from the model. It is also demonstrated that the model provides for further and more comprehensive analysis of the inhibition process, including computing other quantities of interest.

FUNDING

This research project is partially supported by the DST/NRF SARChI Chair on Mathematical Models and Methods in Bioengineering and Biosciences at the University of Pretoria.

DATA AVAILABILITY STATEMENT

All data is graphically represented in Figure 1 (cell viability vs. inhibitor concentration) and in Figure 4 (cell viability vs. time). Numerical values are available from the authors on request.

REFERENCES

- [1] M.-H. Chu, S.-W. Hsiao, Y.-C. Kao, H.-W. Yin, Y.-H. Kuo and C.-K. Lee, Cytotoxicity effect of constituents of *Pinus taiwanensis* Hayata Twigs on B16-F10 melanoma cells. *Molecules* **27** (2022) 2731.
- [2] L. Sun, Z. Li, H. Shang and X. Xin, Hypericin enhances paclitaxel-induced B16-F10 cell apoptosis by activating a cytochrome *c* release-dependent pathway. *Front. Pharmacol.* **12** (2021) 652452.
- [3] W.W. Overwijk and N.P. Restifo, B16 as a mouse model for human melanoma. *Curr. Protoc. Immunol.* **39** (2001) 20.
- [4] P.A. Ott, S. Hu-Lieskovan, B. Chmielowski, R. Govindan, A. Naing, N. Bhardwaj, K. Margolin, M.M. Awad, M.D. Hellmann, J.J. Lin and T. Friedlander, A phase Ib trial of personalized neoantigen therapy plus anti-PD-1 in patients with advanced melanoma, non-small cell lung cancer, or bladder cancer. *Cell* **183** (2020) 347–362.
- [5] R.S. do Nascimento, M.K. Nagamine, G.F. De Toledo, L.M. Chaible, M.V. Tedardi, M.P. Del-Grande, I.I. da Fonseca and M.L. Dagli, Sodium dichloroacetate attenuates the growth of B16-F10 melanoma *in vitro* and *in vivo*: an opportunity for drug repurposing. *Anti-Cancer Drugs* **32** (2021) 111–116.
- [6] B.S. Gomes, J.D. Sousa and R.L. Mendes, Antimelanoma potential of natural compounds derived from plants: a systematic review of *in vivo* studies of B16 melanoma and its sublines. *Braz. J. Med. Biol. Res.* **58** (2025), <https://doi.org/10.1590/1414-431X2025e14480>.
- [7] Z. Ya, Y. Hailemichael, W. Overwijk and N.P. Restifo, Mouse model for pre-clinical study of human cancer immunotherapy. *Curr. Protoc. Immunol.* **108** (2015) 20.1.1–20.1.43.
- [8] N. Cogno, C. Axenie, R. Bauer and V. Vavourakis, Agent-based modeling in cancer biomedicine: applications and tools for calibration and validation. *Cancer Biol. Ther.* **25** (2024) 2344600.
- [9] R. Anguelov, G. Manjunath, A.E. Phiri, T.T. Nyakudya, P. Bipath, J.C. Serem and Y.N. Hlophe, Quantifying assays: inhibition of signalling pathways of cancer. *Math. Med. Biol.* **40** (2023) 266–290.
- [10] C. Basson, A. E. Phiri, G. Manjunath, R. Anguelov, J.C. Serem, P. Bipath and Y.N. Hlophe, *In vitro* effects and mathematical modelling of CTCE-9908 (a chemokine receptor 4 antagonist) on melanoma cell survival. *Clin. Exp. Pharmacol. Physiol.* **51** (2024) e13865.
- [11] V. Kirkin, W. Thiele, P. Baumann, R. Mazitschek, K. Rohde, G. Fellbrich, W. Herbert, J. Waltenberger, A. Giannis and J.P. Sleeman, MAZ51, an indolinone that inhibits endothelial cell and tumor cell growth in vitro, suppresses tumor growth in vivo. *Int. J. Cancer* **112** (2004) 986–993.
- [12] Y.N. Hlophe and A.M. Joubert, Vascular endothelial growth factor-C on the upregulation of chemokine receptor-4 and vascular endothelial growth factor receptor-3 on melanoma and endothelioma adhesion. *J. Cell. Mol. Med.* **26** (2022) 5743–5754.

- [13] R.B. Issaka, S. Oommen, S.K. Gupta, G. Liu, J.L. Myers, J.H. Ryu and N.E. Vlahakis, Vascular endothelial growth factors C and D induces proliferation of lymphangioliomyomatosis cells through autocrine crosstalk with endothelium. *Am. J. Pathol.* **175** (2009) 1410–1420.
- [14] K. Letsoalo, C. Basson, T. Nyakudya and Y. Hlophe, Exploring phytochemical adjuvant therapy in melanoma treatment: The effects of MAZ-51 and zingerone on melanoma cell proliferation. *Clin. Exp. Pharmacol. Physiol.* (In press).
- [15] K. Letsoalo, E. Nortje, S. Patrick, T. Nyakudya and Y. Hlophe, Decoding the synergistic potential of MAZ-51 and zingerone as therapy for melanoma treatment in alignment with the sustainable development goals. *Cell. Biochem. Funct.* **42** (2024) e3950.
- [16] A.M. Jarrett, E.A.B.F. Lima, D.A. Hormuth, II, M.T. McKenna, X. Feng, D.A. Ekrut, A.C.N. Resende, A. Brock and T.E. Yankeelov, Mathematical models of tumor cell proliferation: a review of the literature. *Expert Rev. Anticancer Ther.* **18** (2018) 1271–1286.
- [17] A. Yin, D.J.A.R. Moes, J.G.C. van Hasselt, J.J. Swen and H.-J. Guchelaar, A review of mathematical models for tumor dynamics and treatment resistance evolution of solid tumors. *CPT Pharmacom. Syst. Pharmacol.* **8** (2019) 720–737.
- [18] M. Kohandel, S. Sivaloganathan and A. Oza, Mathematical modeling of ovarian cancer treatments: sequencing of surgery and chemotherapy. *J. Theoret. Biol.* **242** (2006) 62–68.
- [19] H.E. Skipper, F.M. Schabel Jr. and W.S. Wilcox, Experimental evaluation of potential anticancer agents XIII: on the criteria and kinetics associated with curability of experimental leukemia. *Cancer Chemother. Rep.* **35** (1964) 1–111.
- [20] J.C. Panetta, A mathematical model of breast and ovarian cancer treated with paclitaxel. *Math. Biosci.* **146** (1997) 89–113.
- [21] K. Renner-Martin, N. Brunner, M. Kühleitner, W.G. Nowak and K. Scheicher, On the exponent in the Von Bertalanffy growth model. *PeerJ* **6** (2018) e4205.
- [22] R.I. Fletcher, A general solution for the complete Richards function. *Math. Biosci.* **27** (1975) 349–360.
- [23] S.M. Markov, The Gompertz model revisited and modified using reaction networks: mathematical analysis. *Biomath* **10** (2021) 2110023.
- [24] J. West, Z. Hasnain, P. Macklin and P.K. Newton, An evolutionary model of tumor cell kinetics and the emergence of molecular heterogeneity driving gompertzian growth. *SIAM Rev.* **58** (2016) 716–736.
- [25] F.J. Richards, A flexible growth function for empirical use. *J. Exp. Bot.* **10** (1959) 290–300.
- [26] A. Calaprice, *The Ultimate Quotable Einstein*, Princeton University Press, Princeton and Oxford (2011). <https://press.princeton.edu/books/hardcover/9780691138176/the-ultimate-quotable-einstein>.



Please help to maintain this journal in open access!

This journal is currently published in open access under the Subscribe to Open model (S2O). We are thankful to our subscribers and supporters for making it possible to publish this journal in open access in the current year, free of charge for authors and readers.

Check with your library that it subscribes to the journal, or consider making a personal donation to the S2O programme by contacting subscribers@edpsciences.org.

More information, including a list of supporters and financial transparency reports, is available at <https://edpsciences.org/en/subscribe-to-open-s2o>.